CORE
Metadata, citation and similar papers at core.ac.uk
Provided by ePrints@Bangalore University

Solution combustion derived nanocrystalline Zn 2 SiO 4 : Mn phosphors: A spectroscopic view

R. P. Sreekanth Chakradhar, B. M. Nagabhushana, G. T. Chandrappa, K. P. Ramesh, and J. L. Rao

Citation: The Journal of Chemical Physics **121**, 10250 (2004); doi: 10.1063/1.1808420
View online: http://dx.doi.org/10.1063/1.1808420
View Table of Contents: http://scitation.aip.org/content/aip/journal/jcp/121/20?ver=pdfcov
Published by the AIP Publishing

Articles you may be interested in

Doping concentration driven morphological evolution of Fe doped ZnO nanostructures
J. Appl. Phys. **116**, 164315 (2014); 10.1063/1.4900721

Mn-activated Na2SiF6 red and yellowish-green phosphors: A comparative study
J. Appl. Phys. **110**, 063514 (2011); 10.1063/1.3639298

A yellow phosphor K 2 SiF 6 activated by Mn 2 + ions
J. Appl. Phys. **108**, 063506 (2010); 10.1063/1.3481856

Properties of Na 2 SiF 6 : Mn 4 + and Na 2 GeF 6 : Mn 4 + red phosphors synthesized by wet chemical etching
J. Appl. Phys. **105**, 013525 (2009); 10.1063/1.3056375

Electron paramagnetic resonance and luminescent properties of Mn 2 + : MgGa 2 O 4 phosphor
J. Appl. Phys. **98**, 053910 (2005); 10.1063/1.2037210

This article is copyrighted as indicated in the article. Reuse of AIP content is subject to the terms at: http://scitation.aip.org/termsconditions. Downloaded to IP: 128.59.226.54 On: Wed, 10 Dec 2014 01:08:51

HTML ABSTRACT + LINKS

Solution combustion derived nanocrystalline Zn_2SiO_4:Mn phosphors: A spectroscopic view

R. P. Sreekanth Chakradhar[a)]
Department of Physics, Indian Institute of Science, Bangalore-560 012, India

B. M. Nagabhushana and G. T. Chandrappa
Department of Chemistry, Bangalore University, Bangalore-560 001, India

K. P. Ramesh[b)]
Department of Physics, Indian Institute of Science, Bangalore-560 012, India

J. L. Rao
Department of Physics, S. V. University, Tirupati-517 502, India

(Received 20 May 2004; accepted 30 August 2004)

Manganese doped nanocrystalline willemite powder phosphors $Zn_{2-x}Mn_xSiO_4$ ($0.1 \leqslant x \leqslant 0.5$) have been synthesized by a low-temperature initiated, self-propagating, gas producing solution combustion process. The phosphors have been characterized by using x-ray diffraction (XRD), energy dispersive spectroscopy, scanning electron microscopy, Fourier transform infrared spectroscopy (FTIR), electron paramagnetic resonance (EPR), and photo luminescence (PL) spectroscopic techniques. The lattice parameters calculated from XRD confirm that $Zn_{2-x}Mn_xSiO_4$ has a rhombohedral space group $R3H$. The XRD patterns confirm that $Zn_{2-x}Mn_xSiO_4$ phosphor samples undergo a phase transformation from β-willemite to α-willemite phase at 950 °C. The EPR spectra of Mn^{2+} ions exhibit resonance signals at $g \cong 3.24$ and $g \cong 2.02$, with a sextet hyperfine structure centered around $g \cong 2.02$. The EPR signals of Mn^{2+} give a clear indication of the presence of two different Mn^{2+} sites. The magnitude of the hyperfine splitting (A) indicates that the Mn^{2+} is in an ionic environment. The number of spins participating in resonance (N), the paramagnetic susceptibility (χ), and the zero-field splitting parameter (D) have been evaluated as function of x. It is interesting to observe that the variation of N with temperature obeys Boltzmann. The paramagnetic susceptibility is calculated from the EPR data at various temperatures and the Curie constant and Curie paramagnetic temperature was evaluated from the $1/\chi$ versus T graph. The luminescence of Mn^{2+} ion in Zn_2SiO_4 shows a strong green emission peak around 520 nm from the synthesized phosphor particles under UV excitation (251 nm). The luminescence is assigned to a transition from the upper $^4T_1 \rightarrow {}^6A_1$ ground state. The mechanism involved in the generation of a green emission has been explained in detail. The effect of Mn content on luminescence has also been studied. © *2004 American Institute of Physics.* [DOI: 10.1063/1.1808420]

I. INTRODUCTION

Willemite (α-Zn_2SiO_4), with phenacite structure occurs naturally and belongs to the group of orthosilicates.[1] Willemite possesses a wide range of applications such as phosphor host,[2,3] electrical insulators,[4] glazes and pigments,[5,6] and is also an important component in glass ceramics.[7] Mn-activated willemite (Zn_2SiO_4:Mn) is an efficient green phosphor, and it has attracted many researchers for its potential applications to various types of display panels such as plasma display panel (PDP), vacuum fluorescent display (VFD), and field emission display (FED).[8–11] For enhancing the brightness and resolution of these displays, it is important to synthesize phosphors with high quantum efficiency, controlled morphology and small particle sizes, either amorphous or crystalline is of interest. It is also used as a luminescent material for lamp and cathode ray tubes (CRTs) because of its luminescent efficiency and chemical stability.[12] It has also been tested in thin film electroluminescent (EL) devices[13] and medical imaging radiation detectors.[14]

In spite of wide range of applications only limited literature is available on the synthesis and characterization of these materials. Owing to the less attention given in the past and considering its practical importance, the authors decided to extend the studies on the synthesis, characterization, and microstructure of the willemite phosphors. The conventional methods of mechanical mixing of component oxides or precursors and their subsequent reaction at elevated temperatures[12,15] for the preparation of inorganic materials are currently giving way to the newer processing methods with solutions and sols as starting materials. Such starting materials when carefully used, satisfy all the requirements of homogeneity, chemical purity of phases and low processing

[a)]Electronic mail: chakra72@physics.iisc.ernet.in
[b)]Author to whom correspondence should be addressed. Electronic mail: kpramesh@physics.iisc.ernet.in

 © 2004 American Institute of Physics

This article is copyrighted as indicated in the article. Reuse of AIP content is subject to the terms at: http://scitation.aip.org/termsconditions. Downloaded to IP: 128.59.226.54 On: Wed, 10 Dec 2014 01:08:51

temperatures besides fine particle size with uniform size distribution and large surface area of the synthesized phases.[16,17] The other methods like r.f. magnetron sputtering,[12] sol-gel process,[18,19] single polymer precursor route,[20] charge liquid cluster beam technique[21] have also been reported in the literature.

The present work aims to synthesize nanosized crystalline $Zn_{2-x}Mn_xSiO_4$ $(0.1 \leqslant x \leqslant 0.5)$ powder phosphors by a low temperature initiated, self-propagating, gas producing solution combustion process.[22,23] The advantages of solution combustion method includes (a) well crystallized oxides can be obtained at shorter times, (b) it requires little or no further processing such as milling and firing, (c) there is substantial saving of energy as well as cost since the reaction is sustained by heat generated from the chemical reaction between metal nitrates and fuel. The synthesized powders have been characterized by using XRD, EDS, SEM, FTIR, EPR, and PL spectroscopic techniques and the results obtained are discussed in detail.

II. EXPERIMENT

A. Combustion synthesis of willemite phosphors

The starting materials $Zn(NO_3)_2 \cdot 6H_2O$, silica fume (SiO_2 surface area 200 m^2/g) were the source of Zn and Si used for combustion synthesis of willemite phosphor. Diformyl hydrazine ($C_2H_4N_2O_2$, DFH) was used as a fuel for combustion synthesis which was prepared by the reaction of formic acid and hydrazine hydrate as described in the literature.[24] $Mn(NO_3)_2 \cdot 4H_2O$ is used as a source of Mn. All the chemicals used were of Analar grade quality.

B. Calculation of stoichiometry

The stoichiometry of the redox mixture used for the combustion has been calculated using the total oxidizing and reducing valencies of the compounds which serve as numerical coefficients for the stoichiometric balance so that the equivalent ratio (ϕ_e) is unity and the energy released by the combustion is maximum.[25] According to this concept, the valence of C=+4, H=+1, divalent metal ions=+2, trivalent metal ions=+3, and O=−2. The valence of nitrogen is considered to be zero. Based on these considerations, the zinc nitrate has an oxidizing valence of −10 and DFH ($C_2H_4N_2O_2$) a reducing valence of +8. The detailed calculation of stoichiometry has been reported elsewhere.[25]

In the actual synthesis appropriate stoichiometry of $Zn(NO_3)_2 \cdot 6H_2O$ and DFH were dissolved in a minimum quantity of water in a cylindrical petridish (100 mm diameter and 50 mm height) capacity. To this solution fumed silica was added and dispersed well. The heterogeneous redox mixture was rapidly heated by introducing into a muffle furnace maintained at 500±10 °C. The redox mixtures containing the metal nitrates, silica fume and DFH when rapidly heated around 500 °C, dehydrates forming a honeylike gel, which ignites to yield voluminous foamy willemite powder.

Theoretical equations assuming the complete combustion of the redox mixture used for the synthesis of willemite may be written as

$$4Zn(NO_3)_2(aq) + 2SiO_2(s) + 5C_2H_4N_2O_2(aq) \quad (DFH) \rightarrow 2Zn_2SiO_4(s) + 9N_2(g) + 10H_2O(g) + 10CO_2(g). \quad (1)$$

It is interesting to note that the combustion reaction was violent when fused SiO_2 (particle size≈10 μm) was used instead of fumed silica (particle size≈1 μm) as source of silicon. The violent combustion reaction may be due to the noninvolvement of fused SiO_2 with other constituents during combustion because of its large particle size as compared to fumed SiO_2. The dispersed phase (fumed SiO_2) controls the violent reaction as the combustible gases get trapped in the pores of the foam. In the synthesis of Mn-doped samples, $Mn(NO_3)_2 \cdot 4H_2O$ was added along with $Zn(NO_3)_2 \cdot 6H_2O$.

C. Characterization of phosphors

An x-ray powder diffractometer (Philips PW 1050/70) using Cu K_α radiation with a Ni filter was used to estimate the crystallinity of the phases. The surface morphology, distribution of the grains and EDS (energy dispersive spectroscopy) of the samples were examined on a JEOL (JSM-840A) SEM. The FTIR spectral studies have been performed on a Perkin-Elmer spectrophotometer (spectrum 1000) with KBr pellets.

The EPR spectra were recorded at room temperature as well as at different temperatures using a JEOL-FE-1X ESR spectrometer operating in the X-band frequency (≈9.2 GHz) with a field modulation frequency of 100 kHz. The magnetic field was scanned from 0 to 500 mT and the microwave power used was 5 mW. A powdered specimen of 100 mg was taken in a quartz tube for EPR measurements. The EPR spectrum of $Zn_{1.50}Mn_{0.5}SiO_4$ powder phosphor sample was recorded at different temperatures using a variable temperature controller (JES UCT 2AX). A temperature stability of ±1 K was easily obtained by waiting approximately half an hour at the set temperature before recording a spectrum at each temperature. Photoluminescent excitation and emission spectra were recorded with a Shimadzu spectrofluorophoto meter (model RF 510) equipped with a 150 W xenon lamp as an

This article is copyrighted as indicated in the article. Reuse of AIP content is subject to the terms at: http://scitation.aip.org/termsconditions. Downloaded to IP: 128.59.226.54 On: Wed, 10 Dec 2014 01:08:51

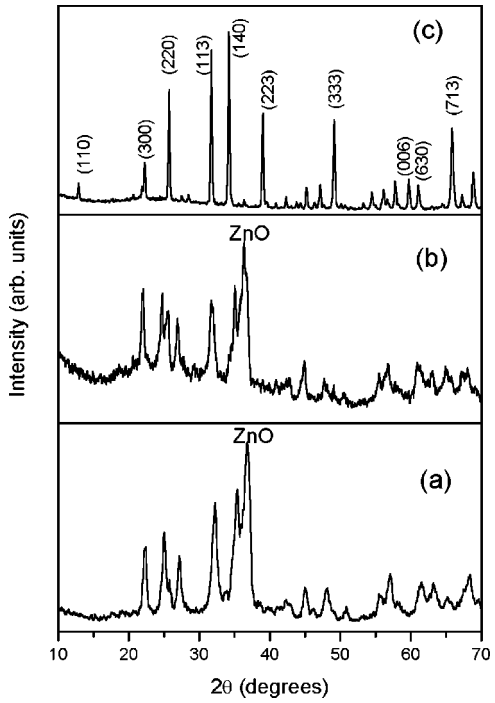

FIG. 1. Powder XRD patterns of solution combustion derived undoped willemite (a) as-formed, (b) 500 °C (3 H), (c) 950 °C (3 H).

excitation source. The emission spectra were studied using an excitation wavelength of 251 nm.

III. RESULTS AND DISCUSSION

The powder x-ray diffraction patterns of undoped and doped willemite phosphors obtained by solution combustion process are shown in Figs. 1 and 2, respectively. The as-formed willemite powder is weakly crystalline with broad peaks corresponding to Zn_2SiO_4 along with ZnO (JCPDS No. 37-7485 and 37-1485) phases. On calcination (950 °C), the powders fully crystallize at the expense of ZnO to give a single phase Zn_2SiO_4 (Fig. 1). Similarly, the Mn doped willemite powders sintered at 950 °C show full crystallinity with small ZnO peak at low Mn doped, but it disappears in high doped powders as shown in Fig. 2. Most intense peaks at $d=2.624$, 2.823, and 3.465 Å do not vary significantly with Mn doping. This suggests crystallinity is therefore independent of Mn content. Table 1 lists the composition and lattice parameters of $Zn_{2-x}Mn_xSiO_4$ $(0.1 \leqslant x \leqslant 0.5)$ phosphors evaluated from the XRD patterns by using Rietveld analysis program Fullprof,[26] assuming the $R3H$ space group. The analysis confirm that these powders have a rhombohedral space group ($R3H$) and are in good agreement with those reported in literature.[27,28] The nominal compositions of the samples were also confirmed by EDS method.

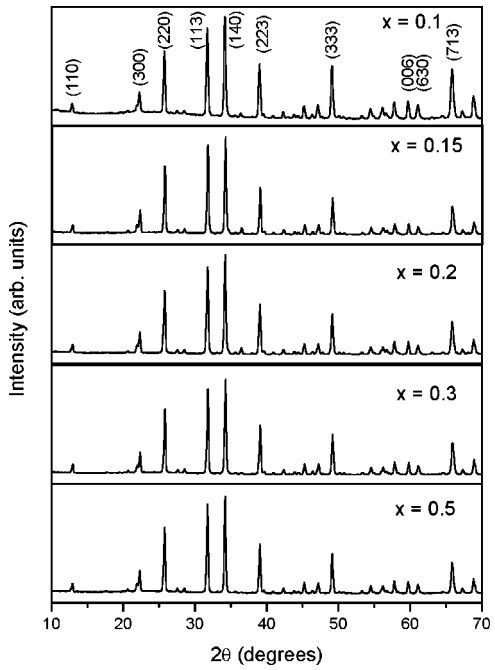

FIG. 2. Powder XRD patterns of solution combustion derived $Zn_{2-x}Mn_xSiO_4$ $(0.1 \leqslant x \leqslant 0.5)$ calcined at 950 °C (3 H) as a function of x.

The SEM micro graphs of $Zn_{2-x}Mn_xSiO_4$ ($x=0.1$ and 0.5) sintered (950 °C) (3 H) samples are shown in Fig. 3. The SEM morphology shows small and round shaped grains which are little bit agglomerated. On calcination the agglomeration size increases. The mean size measured from the scanning electron micrographs is about 0.2–1.2 μm. Also it is well known that the particles prepared using other techniques such as solid state, coprecipitate and hydrothermal are irregular in shape and large.[29–31] The use of spherical shape particles should increase screen brightness and improve the resolution due to lower scattering of the evolved light and higher packing densities than irregular shaped particles.[11]

Using Scherrer's formula,[32] the crystallite size of the samples was calculated from the XRD patterns also. The results show that the particles synthesized in the present investigations are ≈29 to 37 nm.

Figure 4 shows the FTIR spectra of the undoped willemite, as formed and calcined sample (950 °C). It is interesting to observe that as-formed samples exhibit β-willemite phase whereas calcined sample shows α-willemite phase. This also supports our XRD studies (Fig. 1). Figure 5 shows the FTIR spectra of all the doped samples calcined at 950 °C which are in α-willemite phase. It is observed that the main absorption peaks of this phosphor fall in the frequency region 350–1200 cm^{-1}. The IR bands and corresponding vibrational modes for willemite are 870 cm^{-1} (υ_1 SiO_4); 978, 934, and 900 cm^{-1} (υ_3 SiO_4); 460, 396, and 380 cm^{-1} (υ_4 SiO_4); 578 cm^{-1} (υ_1 ZnO_4); and 616 cm^{-1} (υ_3 ZnO_4), where υ_1 corresponds to totally sysmmetric stretching, υ_3 is asymmetric stretching and υ_4 asymmetric deformation.[23,33,34] The absorption at 470 cm^{-1} corresponds to ZnO stretching[35] and it is observed that the intensity of this absorption increases with increase of Mn content.

A. Electron paramagnetic resonance studies

The EPR spectroscopy has been used as a tool to elucidate the structural evolution of the materials. We used divalent Mn as a probe; Mn^{2+} is a sensitive indicator of structural changes owing to its unshielded d^5 ions. Host-activator compositions are of considerable interest for elucidating the structure and bonding in vitreous (isotropic) and crystalline (anisotropic) systems. In undoped samples we have not ob-

This article is copyrighted as indicated in the article. Reuse of AIP content is subject to the terms at: http://scitation.aip.org/termsconditions. Downloaded to IP: 128.59.226.54 On: Wed, 10 Dec 2014 01:08:51

TABLE I. Composition and lattice parameters of $Zn_{2-x}Mn_xSiO_4$ ($0.1 \leqslant x \leqslant 0.5$) phosphors ($R$=rhombohedral; @ accurate within ± 0.009).

Sample	Crystal structure	Lattice parameters (Å)@		Cell volume (Å^3)
		a	c	
$Zn_{1.90}Mn_{0.1}SiO_4$	$R\bar{3}H$	13.947(7)	9.314(3)	1569.08(13)
$Zn_{1.85}Mn_{0.15}SiO_4$	$R\bar{3}H$	13.953(6)	9.317(2)	1570.85(10)
$Zn_{1.8}Mn_{0.2}SiO_4$	$R\bar{3}H$	13.951(5)	9.316(2)	1570.28(10)
$Zn_{1.75}Mn_{0.25}SiO_4$	$R\bar{3}H$	13.948(6)	9.314(2)	1569.48(08)
$Zn_{1.7}Mn_{0.3}SiO_4$	$R\bar{3}H$	13.944(5)	9.312(2)	1568.05(10)
$Zn_{1.5}Mn_{0.5}SiO_4$	$R\bar{3}H$	13.946(5)	9.315(2)	1568.98(08)

served EPR signal indicating that the starting materials used in the present work are free from paramagnetic impurities.

Figure 6 shows the EPR spectra of Mn^{2+} doped $Zn_{2-x}Mn_xSiO_4$ ($0.1 \leqslant x \leqslant 0.5$) phosphors as a function of x. The EPR spectra of all the investigated samples exhibit a six-line hyperfine structure centered at $g \cong 2.02$ with a total peak width of $\cong$490 G as shown in Fig. 6. The six-line hyperfine structure (hfs) arising at $g \cong 2.02$ is due to the interaction of electron spin of manganese ions with its own nuclear spin $I=5/2$. In addition to this, a broad shoulder around $g \cong 3.24$ has also been observed. The observation of EPR signals of Mn^{2+} give a clear indication of two kinds of Mn^{2+} sites. Therefore the EPR spectrum of Mn^{2+} ions is due to isolated Mn^{2+} ions giving the six-line hyperfine structure plus a very broad line due to dipolar interaction between $Mn^{2+}-Mn^{2+}$ neighbors. An EPR study of Mn doped willemite by Perkins and Sienko[36] also indicated that both sites are accessible to Mn^{2+}.

Bulk Zn_2SiO_4:Mn (at 950 °C) crystallizes in phenacite structure and belongs to rhombohedral space group as both Zn^{2+} and Si^{4+} ions coordinated tetrahedrally to four oxygen atoms. There are two nonequivalent crystallographic Zn sites present in willemite both having nearest neighboring oxygen in a slightly distorted tetrahedral (T_d) configuration. Both sites are accessible to Mn^{2+}, since ionic radii of the two ions are very similar (0.74 Å for Zn^{2+} and 0.80 Å for Mn^{2+}) and also due to the identical valency. Therefore the Mn ions doped Zn_2SiO_4 also have four-coordination (weak crystal field) because they replace some of the Zn^{2+} ions in the lattice.[2]

From EPR spectra, the spin-Hamiltonian parameters g and A have been evaluated. Table 2 gives some typical values of the hyperfine splitting (A) values for the $Zn_{2-x}Mn_xSiO_4$ ($0.1 \leqslant x \leqslant 0.5$) phosphors as a function of x at room temperature. It is apparent from different average values of A measured from peak to peak (A_{pp}) and trough to trough (A_{tt}) that the individual lines are strain broadened, leading to an asymmetry in the absorption spectrum.[37] The

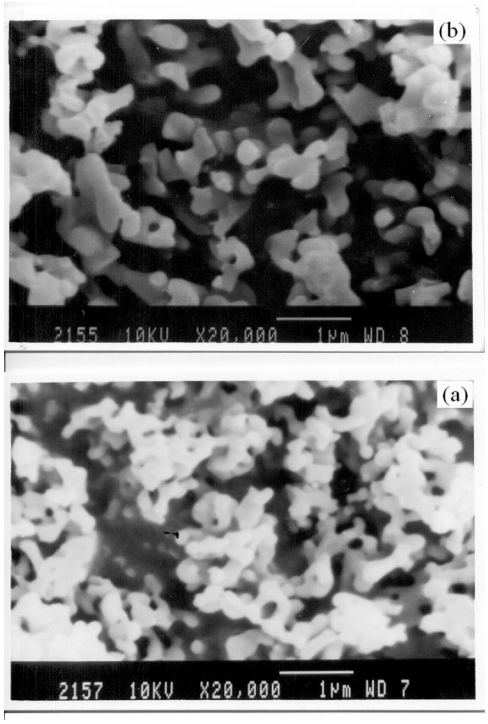

FIG. 3. The SEM morphology of solution combustion derived $Zn_{2-x}Mn_xSiO_4$ samples calcined at 950 °C (3 H) (a) $x=0.1$, (b) $x=0.5$.

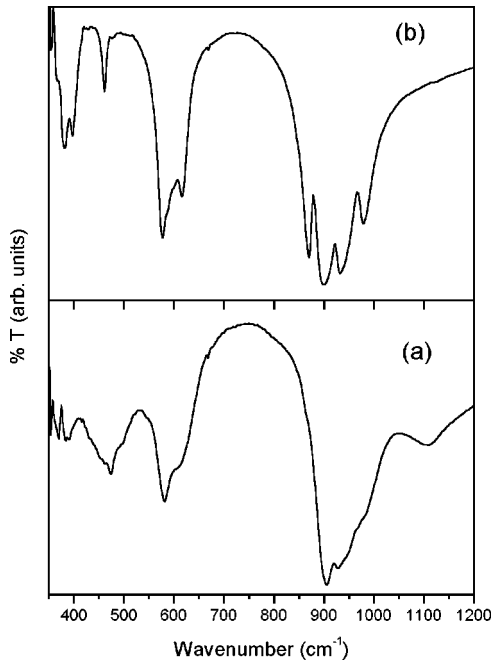

FIG. 4. FTIR spectra of the solution combustion derived undoped willemite powders (a) as-formed and (b) calcined at (950 °C) (3 H).

This article is copyrighted as indicated in the article. Reuse of AIP content is subject to the terms at: http://scitation.aip.org/termsconditions. Downloaded to IP: 128.59.226.54 On: Wed, 10 Dec 2014 01:08:51

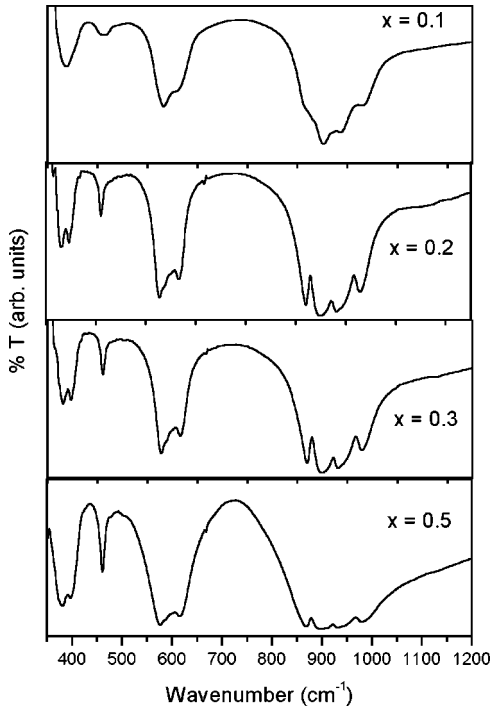

FIG. 5. FTIR spectra of the solution combustion derived $Zn_{2-x}Mn_xSiO_4$ ($0.1 \leqslant x \leqslant 0.5$) calcined at 950 °C (3 H) as a function of x.

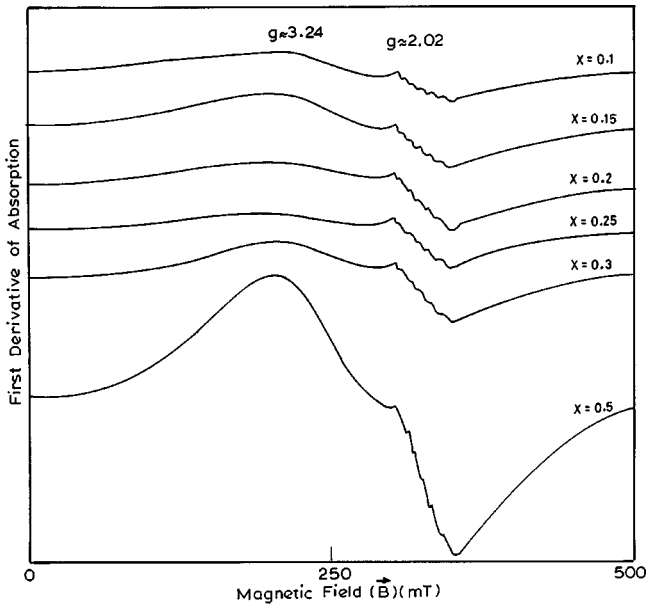

FIG. 6. The X-band EPR spectra of $Zn_{2-x}Mn_xSiO_4$ ($0.1 \leqslant x \leqslant 0.5$) phosphor samples as a function of x at room temperature.

first derivative spectrum as a consequence, shows larger values of A, when measured trough to trough, rather than peak to peak. An overall average was calculated from

$$A_{\text{avg}} = [(\Delta_{\text{Opp}} + \Delta_{\text{Ott}})/5 + (\Delta_{\text{Mpp}} + \Delta_{\text{Mtt}})/3 + (\Delta_{\text{Ipp}} + \Delta_{\text{Itt}})]/6, \quad (2)$$

where Δ_{Opp} and Δ_{Ott} represent the differences between the first and sixth peak positions, measured peak to peak and trough to trough respectively. Δ_{Mpp} and Δ_{Mtt} represents difference in positions between second and fifth peaks and Δ_{Ipp} and Δ_{Itt} between second and third peaks. It is interesting to note that, in all of the samples, $\Delta_{\text{Opp}}/5 \approx \Delta_{\text{Mpp}}/3 \approx \Delta_{\text{Ipp}}$ and $\Delta_{\text{Ott}}/5 \approx \Delta_{\text{Mtt}}/3 \approx \Delta_{\text{Itt}}$. This indicates that the g value in each case is well behaved.[37]

The strength of the hyperfine splitting (A) depends on the matrix into which the ion is dissolved and is mainly determined by the electronegativity of the neighbors. This means a qualitative measure of the covalency of the bonding in the matrix which can be determined from the value of A; the smaller the splitting, the more covalent the bonding of the anion. The g value for the hyperfine splitting is indicative of the nature of bonding in the matrix. If the g value shows a negative shift with respect to 2.0023, then the bonding is ionic and conversely, if the shift is positive, then the bonding is more covalent in nature. In the present work, from the measured negative shift in the g value, with respect to 2.0023 as well as from A values, it is apparent that the Mn^{2+} ion is in an ionic environment. It is also observed that the linewidth, and g and A values are found to be independent of temperature.

B. Calculation of number of spins (N) participating in resonance

The number of spins participating in resonance can be calculated by comparing the area under the absorption curve with that of a standard ($CuSO_4 \cdot 5H_2O$ in this study) of known concentration. Weil *et al.*[38] gave the following expression which includes the experimental parameters of both sample and standard:

TABLE II. The hyperfine splitting (A), number of spins participating in resonance (N), paramagnetic susceptibility (χ) and zero-field splitting parameter (D) for ($Zn_{2-x}Mn_xSiO_4$) ($0.1 \leqslant x \leqslant 0.5$) as a function of x at room temperature.

Sample ($Zn_{2-x}Mn_xSiO_4$)	A_{avg} $\times 10^{-4}$ cm^{-1}	$N \times 10^{20}$ (arbitrary units)	$\chi \times 10^{-4}$ (m^3 Kg^{-1})	D (Gauss)
$x = 0.10$	75.1	7.44	1.87	227
$x = 0.15$	74.8	11.75	2.95	232
$x = 0.20$	75.5	17.36	4.36	234
$x = 0.25$	78.3	19.67	4.94	247
$x = 0.30$	74.1	20.24	5.08	258
$x = 0.50$	75.2	45.83	11.5	268

This article is copyrighted as indicated in the article. Reuse of AIP content is subject to the terms at: http://scitation.aip.org/termsconditions. Downloaded to IP: 128.59.226.54 On: Wed, 10 Dec 2014 01:08:51

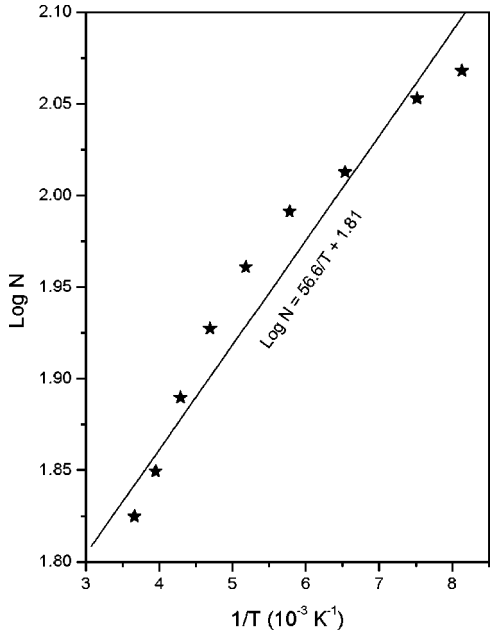

FIG. 7. A plot of $\ln N_{g=2.02}$ against $1/T$ for the $Zn_{1.5}Mn_{0.5}SiO_4$ powder phosphor sample.

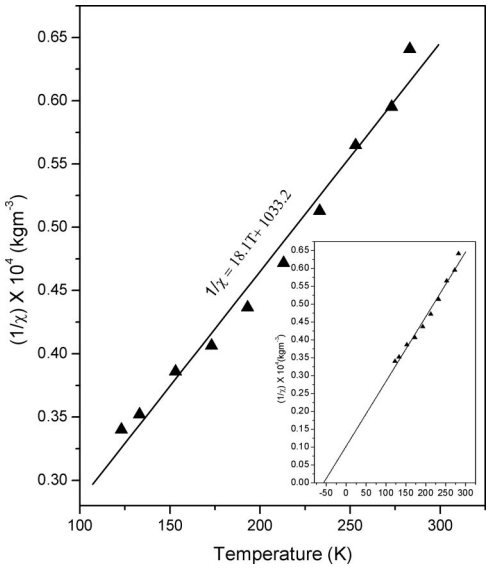

FIG. 8. The variation of reciprocal of paramagnetic susceptibility $(1/\chi)$ as a function of absolute temperature (T) for the $Zn_{1.5}Mn_{0.5}SiO_4$ powder phosphor sample.

$$N = \frac{A_x(Scan_x)^2 G_{\text{std}}(B_m)_{\text{std}}(g_{\text{std}})^2[S(S+1)]_{\text{std}}(P_{\text{std}})^{1/2}}{A_{\text{std}}(Scan_{\text{std}})^2 G_x(B_m)_x(g_x)^2[S(S+1)]_x(P_x)^{1/2}} \times[\text{Std}], \tag{3}$$

where A is the area under the absorption curve which can be obtained by double integrating the first derivative EPR absorption curve, *scan* is the magnetic field corresponding to unit length of the chart, G is the gain, B_m is the modulation field width, g is the g factor, S is the spin of the system in its ground state. P is the power of the microwave. The subscripts "x" and "Std" represent the corresponding quantities for Mn^{2+} glass sample and the reference $(CuSO_4 \cdot 5H_2O)$, respectively. It is observed that the number of spins participating in resonance for $g \cong 2.02$ increase with x and is presented in Table 2. This increase in N is due to more number of Mn content is entering the matrix as a paramagnetic impurity. Figure 7 shows a plot of $\ln N_{g=2.02}$ against $1/T$ in 100 mg of the powder phosphor sample $Zn_{1.5}Mn_{0.5}SiO_4$. From the plot it can be seen that, as the temperature is lowered the number of spins increases obeying the usual Boltzmann law. The data is least square fit to a straight line $\ln N = (56.6/T) + 1.81$. The activation energy thus calculated was found to be 1.798×10^{-21} J (0.0112 eV) which is the same order expected for a paramagnetic ion.

C. Calculation of paramagnet ic susceptibility (χ) from EPR data

The EPR data can be used to calculate the paramagnetic susceptibility of the sample using the formula,[39]

$$\chi = \frac{Ng^2\beta^2 \text{J(J+1)}}{3k_B(T+\Delta)}, \tag{4}$$

where N is the number of spins per m^3 and the other symbols have their usual meaning. When Weiss constant Δ vanishes, Eq. (4) follows Curie's law. N can be calculated from Eq. (3) and $g = 2.02$ is taken from EPR data. The paramagnetic susceptibility have also been evaluated with respect to x and is presented in Table 2. The temperature dependence of reciprocal of the paramagnetic susceptibility $(1/\chi)$ of Mn^{2+} ions in $Zn_{1.5}Mn_{0.5}SiO_4$ phosphor sample is presented in Fig. 8. The data is fit to a straight line in accordance with Curie-Weiss-type behavior $[\chi = C/(T-\theta_p)]$. It is interesting to note that with increasing temperature, the susceptibility of the sample decreases obeying the Curie-Weiss law. Further from the slope of the line the Curie constant and the paramagnetic Curie temperature have been evaluated and are found to be 55.23×10^{-3} emu mol^{-1} and $\theta_p = -55$ K, respectively. The Curie constant calculated in the present work is in good agreement with the value reported for the paramagnetic ion by Ardelean *et al.*[40] The paramagnetic Curie temperature is negative for the investigated sample implying that the manganese ions are antiferromagnetically coupled by negative super exchange interactions at very low temperatures.

D. Calculation of zero-field splitting parameter (D) from EPR spectra from the allowed hyperfine lines

The intensity of hyperfine lines can be used to calculate the zero-field splitting parameter (D) from the ratio of allowed hyperfine lines (corresponding to the selection rule $\Delta m = 0$) using the formula[41]

$$I_m \propto 2\frac{A^2(35-4m^2)}{2(g\beta H)^2} - \frac{5.334D^2}{(g\beta H)^2} - \frac{35.14D^2(35-4m^2)}{(g\beta H)^2} + \frac{208D^4(35-4m^2)^2}{(g\beta H)^4}, \tag{5}$$

This article is copyrighted as indicated in the article. Reuse of AIP content is subject to the terms at: http://scitation.aip.org/termsconditions. Downloaded to IP: 128.59.226.54 On: Wed, 10 Dec 2014 01:08:51

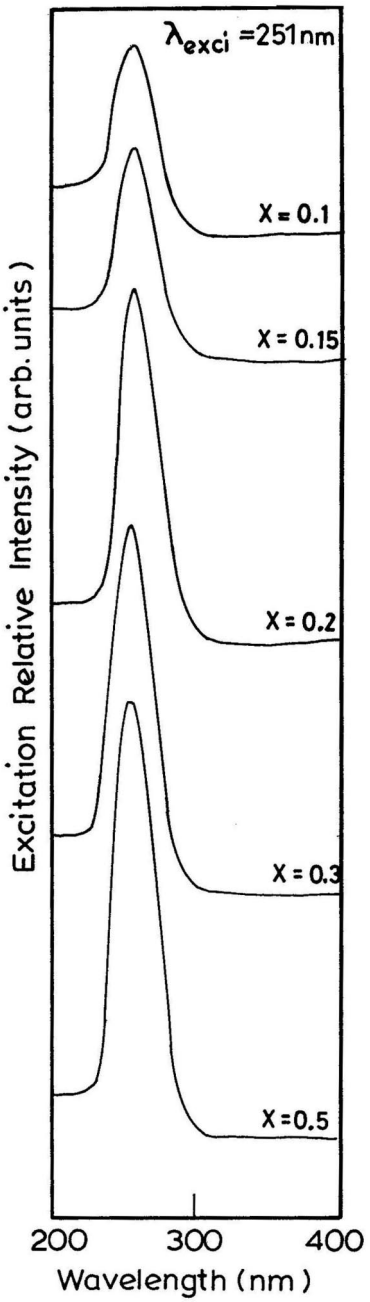

FIG. 9. The excitation spectra taken at the peak emission (≈520 nm) at room temperature in solution combustion derived $Zn_{2-x}Mn_xSiO_4$ ($0.1 \leqslant x \leqslant 0.5$) calcined at 950 °C (3 H) as a function of x.

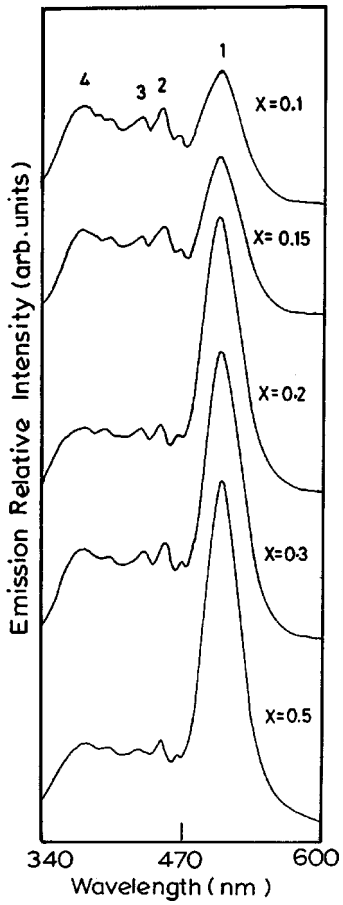

FIG. 10. Emission spectra of phosphor particles at room temperature in solution combustion derived $Zn_{2-x}Mn_xSiO_4$ ($0.1 \leqslant x \leqslant 0.5$) samples calcined at 950 °C (3 H) as a function of x under an excitation of 251 nm.

where m is the nuclear spin magnetic quantum number, I_m is the intensity of the mth allowed hyperfine (HF) line, A is the HF splitting constant, D is the zero-field splitting parameter, and the rest of the symbols have their usual meaning. The D values evaluated in the present work is listed in Table 2. It is observed that D increases with x.

IV. PHOTOLUMINESCENCE STUDIES

The photoluminescence (PL) of $Zn_{2-x}Mn_xSiO_4$ ($0.1 \leqslant x \leqslant 0.5$) phosphors have been characterized by the transitions of $3d^5$ of Mn^{2+} electrons in the manganese ion acting as an activating center. In a cubic crystalline field of low to moderate strength, the five d electrons of Mn^{2+} ion are distributed in the t_{2g} and e_g orbitals, with three in the former and two in the latter. Thus the ground state configuration is $(t_{2g})^3(e_g)^2$. This configuration gives rise to the electronic states, $^6A_{1g}$, $^4A_{1g}$, ^4E_g, $^4T_{1g}$, $^4T_{2g}$, and to a number of doublet states of which $^6A_{1g}$ lies lowest according to Hund's rule. Since, all the excited states of Mn^{2+} ion (belonging to d^5 configuration) will be either quartets or doublets, the luminescence spectra of Mn^{2+} ions will have only spin forbidden transitions.

Figure 9 shows an excitation spectrum of $Zn_{2-x}Mn_xSiO_4$ ($0.1 \leqslant x \leqslant 0.5$) phosphor with a strong excitation peak at 251 nm, obtained by monitoring the strong green emission wavelength at 520 nm (see Fig. 9) or the band at 251 nm is considered to be responsible for the emission at 520 nm. The broad strong excitation peak at 251 nm could be attributed to a charge transfer transition from the divalent manganese ground state $^6A_1(S)$ of (Mn^{2+}) to the conduction band (CB). The corresponding emission spectra of Zn_2SiO_4:Mn ($0.1 \leqslant x \leqslant 0.5$) phosphor is shown in Fig. 10. In the present work we observed interesting new results. In addition to strong green emission (520 nm), we also observed weak blue (430–460 nm) and violet (390 nm) emissions from the same material for a single excitation wavelength of 251 nm. To the best of our knowledge we have not come across such an emission spectra consisting of three wavelengths simultaneously in this series of Zn_2SiO_4:Mn phos-

This article is copyrighted as indicated in the article. Reuse of AIP content is subject to the terms at: http://scitation.aip.org/termsconditions. Downloaded to IP: 128.59.226.54 On: Wed, 10 Dec 2014 01:08:51

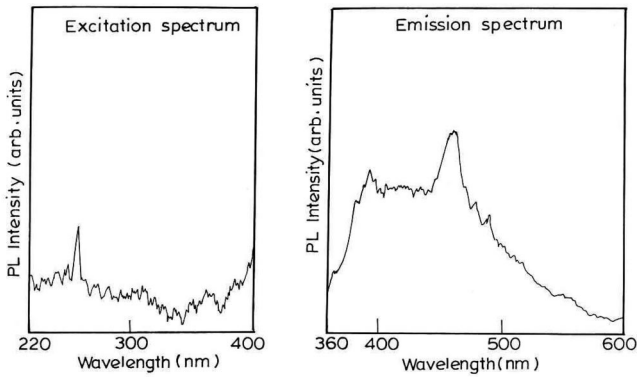

FIG. 11. The excitation and emission spectra of undoped solution combustion derived willemite sample calcined at 950 °C (3 H).

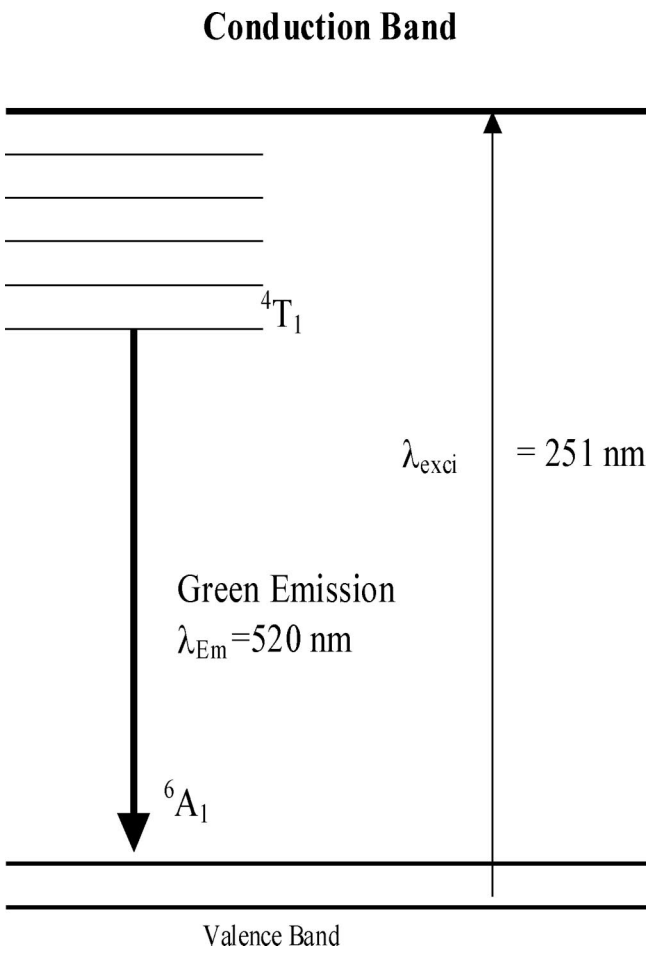

FIG. 12. Energy level scheme for the green emission process in $Zn_{2-x}Mn_xSiO_4$ $(0.1 \leqslant x \leqslant 0.5)$ samples upon excitation with 251 nm of Xe lamp.

phors reported so far. Most of the available reports indicate only green emission. In order to probe for the origin of additional colors in the emission spectra we have performed PL studies in undoped samples also.

Surprisingly the PL spectra of undoped samples also showed very weak two emission peaks at about 395 nm (UV band) and 465 nm (blue band) from emission spectra when excited at 260 nm. The excitation and emission spectra of undoped sample is shown in Fig. 11 and the absence of green emission is due to the absence of Mn^{2+}. Further our EPR experiment in undoped sample also shows the absence of EPR signal, indicating that it is free from paramagnetic impurities. Therefore, we attribute these additional bands in our samples at about ~390 and ~460 nm to be originating from ZnO. The UV emission at ~390 nm has been well studied and was ascribed to excitonic recombination of ZnO. It is well known[42] that the valence band (VB) and CB in semiconductors retain their meaning even in the amorphous state, and the density of bands is almost unaltered by amorphisation since the gross feature of electronic states is determined by the short range order. The photophysics of emission band at ~390 nm can be predicted by the following scheme: First, the excitation photon may lose energy of ~2 eV due to vibrational absorption in the silica network before exciting the electron from VB to CB of ZnO. A similar energy loss process is reported in porous silica.[43] Second, the excited electrons move towards the band edge and recombine directly with the photogenerated holes to give the 390 nm emission. For different syntheses approaches, the near band edge emission peaked at ~380 nm was also reported.[44–47]

Blue light luminescence located at 430–460 nm has been reported by Fu *et al.*[48] in their ZnO films deposited on a Si substrate. Similarly, a very weak 470 nm blue emission peak was reported by Li *et al.*[49] in their ZnO/Zn phosphor films. Only a few results[48–52] on this emission have been reported and its mechanism is still being debated. Zhang *et al.*[52] reported monochromatic blue luminescence from sputtered ZnO films and ascribed it to shallow donor level of oxygen vacancy and interstitial zinc. Other possible origins such as zinc vacancy[48] and interstitial oxygen[50] have also been proposed to explain this blue emission. Zhang *et al.* reported that a 446 nm blue emission was observed in their ZnO films deposited on a glass substrate[52] when exited with a 270 nm light.

Recently Xu *et al.*[53] reported a new evidence for 453 nm blue band by resolving the unsymmetric UV band of the annealed ZnO film in their study of formation mechanism of Zn_2SiO_4 crystal. They also pointed out that the 453 nm blue luminescence is from an unknown blue center and they reasonably attributed these blue centers in the α-SiO_2 to the ZnO film deposited on silicon.

In the present investigations interestingly we observed all the features described above in our samples, especially the green, blue, and violet emissions with a single excitation wavelength. The intensities of the blue and violet are weak compared to strong green emission. In undoped samples the green emission was absent, hence we deduce that the strong green photoemission originates from Mn^{2+}. Therefore, in this study the strong green light emitted from the Mn^{2+} doped Zn_2SiO_4 phosphor particles under UV excitation and has been assigned to an electronic transition of $^4T_1(G) \rightarrow {}^6A_1(S)$ peaking at the wavelength 520 nm and which is parity forbidden emission transition of Mn^{2+} ions.[54] The Mn^{2+} ion site substituting the Zn^{2+} in the Zn_2SiO_4 lattice is considered to be the emission center of the Zn_2SiO_4:Mn phosphor because Zn^{2+} and Mn^{2+} ions have similar oxidation states and their radii are similar; therefore Mn^{2+} ions

This article is copyrighted as indicated in the article. Reuse of AIP content is subject to the terms at: http://scitation.aip.org/termsconditions. Downloaded to IP: 128.59.226.54 On: Wed, 10 Dec 2014 01:08:51

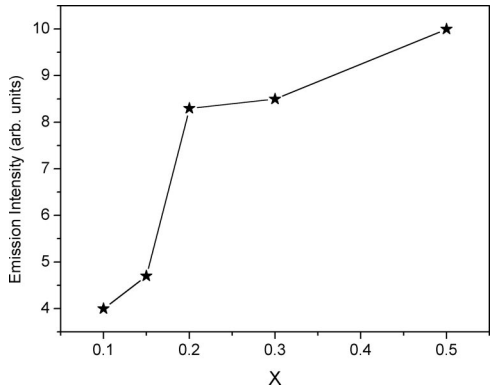

FIG. 13. Green color (520 nm) emission dependence in $Zn_{2-x}Mn_xSiO_4$ ($0.1 \leqslant x \leqslant 0.5$) samples as a function of x upon excitation with 251 nm of Xe lamp.

could be well distributed as the substitutes of Zn^{2+} in the zinc silicate host matrix and hence the encouraging green emission. The valence matching between Mn and Zn could lead to a high solid solubility even at low temperatures without any charge compensators.[55] The mechanism involved in the generation of a green emission in this system is shown in Fig. 12. The electron from the ground state of Mn^{2+} ($^6A_1$) is excited to the conduction band of the Zn_2SiO_4 by photons. This process may be explained as

$$Mn^{2+} + h\nu \rightarrow Mn^{3+} + e^-,$$

where $h\nu$ is the energy needed in causing the photoexcitation of Mn^{2+} in Zn_2SiO_4. The free electrons in the conduction band can relax to the $^4T_1$ excited state by nonradiative process and then followed by radiative transition from the excited state $^4T_1 \rightarrow {}^6A_1$ ground state emitting a strong green light.

The brightness of the emission from the phosphor particles is strongly affected by doping concentration of Mn^{2+}. The dependence of emission intensity with doping is shown in Fig. 13. It is observed that the emission intensity increases linearly with Mn content up to $x=0.2$; afterwards it begins to saturate. The dependence of emission intensity on Mn content has also been reported in literature.[56–62] In the present investigation the origin of blue and violet emissions are not clear. However, it is reasonable to attribute this to the fact that it may be originating from the zinc vacancy.

V. CONCLUSIONS

$Zn_{2-x}Mn_xSiO_4$ ($0.1 \leqslant x \leqslant 0.5$) nanocrystalline powder phosphors have been synthesized by a low-temperature initiated, self-propagating, gas producing combustion process. The lattice parameters calculated from XRD confirm that $Zn_{2-x}Mn_xSiO_4$ has a rhombohedral space group ($R3H$). The XRD patterns confirm that $Zn_{2-x}Mn_xSiO_4$ phosphor samples undergo a phase transformation from β-willemite to α-willemite phase at 950 °C. The EPR spectra of Mn^{2+} ions exhibit resonance signals at $g \cong 3.24$ and $g \cong 2.02$, with a sextet hyperfine structure centered around $g \cong 2.02$. The observation of EPR signals of Mn^{2+} gives clear indication of two kinds of Mn^{2+} sites. The magnitude of hyperfine splitting (A) for Mn^{2+} ion indicates that the Mn^{2+} ion is in an ionic environment. It is observed that N, χ, and D increases with increase of x. The variation of N with temperature obeys usual Boltzmann law. The activation energy was calculated and found to be 0.0112 eV. It is interesting to observe that the temperature dependence of reciprocal of susceptibility obeys Curie-Weiss law. The Mn ions in doped Zn_2SiO_4 also have four-coordination because they replace some of the Zn^{2+} ions in the lattice. The luminescence of Mn^{2+} ion in Zn_2SiO_4 shows a strong green emission peak around 520 nm from the synthesized phosphor particles under UV excitation (251 nm). The luminescence is assigned to a transition from the upper $^4T_1 \rightarrow {}^6A_1$ ground state. In addition to this, blue and violet emissions are also observed for single excitation wavelength (251 nm). The origin for green emission is from Mn^{2+} center, whereas blue and violent emissions may be originating from the zinc vacancy.

ACKNOWLEDGMENTS

The authors thank DST, DAE-BRNS for providing financial assistance. R.P.S.C. is grateful to the Science and Engineering Research Council SERC (Department of Science and Technology, DST), New Delhi, for the award of Fast Track research project under Young scientist scheme.

[1] J. A. Speer and P. H. Ribbe, in *Reviews in Mineralogy*, 2nd ed., edited by P. H. Ribbe (Mineralogical Society of America, Washington, DC, 1982), Vol. 5, p. 429.
[2] K. C. Mishra, K. H. Johnson, B. G. Deboer, J. K. Berkowitz, J. Olsen, and E. A. Dale, J. Lumin. **47**, 197 (1991).
[3] C. Bartohu, J. Benoit, P. Bennalloul, and A. Morell, J. Electrochem. Soc. **141**, 524 (1994).
[4] D. Lepkova, A. Nenov, L. Pavlova, and I. Ivalnov, Stroit. Materi. Silik. Promst. **21**, 18 (1980).
[5] J. Alarcon, P. Escribano, and R. Maria Martin, Br. Ceram. Trans. J. **84**, 170 (1985).
[6] E. Rosello, A. Borrio, M. Guillem, and M. Cormen, Br. Ceram. Trans. J. **84**, 175 (1985).
[7] Z. Strand, *Glass Science and Technology* (Elsevier, Amsterdam, 1986), Vol. 8, p. 101.
[8] J. McKittrick, L. E. Shea, C. F. Bacalski, and E. J. Bosze, Displays **19**, 169 (1999).
[9] Y. C. Kang, I. W. Lenggoro, S. B. Park, and K. Okuyama, J. Phys. Chem. Solids **60**, 1855 (1999).
[10] L. E. Shea, J. McKittrick, and O. A. Lopez, J. Am. Ceram. Soc. **79**, 3257 (1996).
[11] *Phosphor Handbook*, edited by S. Shionoya and W. M. Yen, Phosphor Research Society (Japan) (CRC, Boca Raton, FL, 1999).
[12] H. C. Swart, T. A. Trottier, J. S. Sebastian, S. L. Jones, and P. H. Holloway, J. Appl. Phys. **83**, 4578 (1998).
[13] T. Minami, T. Miyata, S. Takata, and I. Fukuda, Jpn. J. Appl. Phys., Part 2 **30**, L117 (1991).
[14] I. Kandarakis, D. Cavouras, P. Prassopoulos, E. Kanellopoulos, C. D. Nomicos, and G. S. Panayiotakis, Appl. Phys. A: Mater. Sci. Process. **67**, 521 (1998).
[15] D. Segal, *Chemical Synthesis of Advanced Ceramic Materials* (Cambridge University Press, Cambridge, 1989).
[16] C. R. Veale, *Fine Powders: Preparation, Properties and Uses* (Applied Science Publishers, London, 1972).
[17] K. S. Sohn, B. Cho, and H. D. Park, J. Am. Ceram. Soc. **82**, 2779 (1999).
[18] R. Morimo and K. Matae, Mater. Res. Bull. **24**, 175 (1989).
[19] J. Lin, U. D. Sanger, M. Menning, and K. Barner, Mater. Sci. Eng., B **64**, 73 (1999).
[20] K. Su, T. D. Tilley, and M. J. Sailor, J. Am. Ceram. Soc. **118**, 3459 (1996).
[21] M. Cich, K. Kim, H. Choi, and S. T. Hwang, Appl. Phys. Lett. **73**, 2116 (1998).
[22] J. J. Kingsley and K. C. Patil, Mater. Lett. **6**, 427 (1998).

This article is copyrighted as indicated in the article. Reuse of AIP content is subject to the terms at: http://scitation.aip.org/termsconditions. Downloaded to IP: 128.59.226.54 On: Wed, 10 Dec 2014 01:08:51

[23] G. T. Chandrappa, S. Ghosh, and K. C. Patil, J. Mater. Synth. Process. **7**, 273 (1999).
[24] C. Ainsworth and R. Jones, J. Am. Ceram. Soc. **77**, 621 (1955).
[25] S. R. Jain, K. C. Adiga, and V. R. Paiverneker, Combust. Flame **40**, 71 (1981).
[26] J. Rodriguez-Carvajal, Program Fullprof. **98**, version 0.2 (1998).
[27] R. W. G. Wyckoff, Cryst. Struct. Commun. **3**, 134 (1963).
[28] T. S. Ahmadi, M. Haase, and H. Weller, Mater. Res. Bull. **35**, 1869 (2000).
[29] I. F. Chang, J. W. Brownlow, T. I. Sun, and J. S. Wilson, J. Electrochem. Soc. **136**, 3532 (1989).
[30] A. Morell and N. El Khiati, J. Electrochem. Soc. **140**, 2019 (1993).
[31] Q. H. Li, S. Komarneni, and R. Roy, J. Mater. Sci. **30**, 2358 (1995).
[32] H. Klug and L. Alexander, *X-ray Diffraction Procedures for Polycrystalline and Amorphous Materials* (Wiley, New York, 1974), p. 618.
[33] P. Tarte, Spectrochim. Acta **18**, 467 (1962).
[34] C.-C. Lin and P. Shen, J. Non-Cryst. Solids **171**, 281 (1994).
[35] R. A. Nyquist and R. O. Kagel, *Infrared Spectra of Inorganic Compounds* (Academic, New York, 1971).
[36] H. K. Perkins and M. J. Sienko, J. Chem. Phys. **46**, 2398 (1967).
[37] J. R. Pilbrow, Bull. Magn. Reson. **9**, 32 (1987).
[38] J. A. Weil, J. R. Bolton, and J. E. Wertz, *Electron Paramagnetic Resonance-Elementary Theory and Practical Applications* (Wiley, New York, 1994), p. 498.
[39] N. W. Aschcroft and N. D. Mermin, *Solid State Physics* (Harcourt Brace College Publishers, New York, 2001), p. 656.
[40] I. Ardelean, O. Cozar, S. Filip, V. Pop, and I. Ceran, Solid State Commun. **100**, 609 (1996).
[41] B. T. Allen, J. Chem. Phys. **43**, 3820 (1965).
[42] S. Kondo, T. Itoh, and T. Saito, Phys. Rev. B **57**, 13235 (1998).
[43] B. D. Yao, H. Z. Shi, X. Y. Zhang, and L. D. Zhang, Appl. Phys. Lett. **78**, 174 (2001).
[44] Z. K. Tang, G. K. L. Wong, P. Yu, M. Kawasaki, A. Ohtomo, H. Koinuma, and Y. Segawa, Appl. Phys. Lett. **72**, 3270 (1998).
[45] M. H. Huang, Y. Wu, H. Feick, N. Tran, E. Weber, and P. Yang, Adv. Funct. Mater. **13**, 113 (2001).
[46] Y. C. Kong, D. P. Yu, B. Zhang, W. Fang, and S. Q. Feng, Appl. Phys. Lett. **78**, 407 (2001).
[47] M. H. Huang, S. Mao, H. Feick *et al.*, Science **292**, 1897 (2001).
[48] Z. X. Fu, C. X. Guo, B. X. Lin, and G. H. Liao, Chin. Phys. Lett. **15**, 457 (1998).
[49] W. Li, D. S. Mao, Z. H. Zheng *et al.*, Surf. Coat. Technol. **129–129**, 346 (2000).
[50] M. Shailaja, B. Kavita, B. S. Bendre, V. J. Leppert, and S. H. Risbud, J. Appl. Phys. **85**, 2861 (1999).
[51] T. Gao, G. W. Meng, Y. T. Tian, S. H. Sun, X. Liu, and L. D. Zhang, J. Phys.: Condens. Matter **14**, 12651 (2002).
[52] D. H. Zhang, Z. Y. Xue, and Q. P. Wang, J. Phys. D **35**, 2837 (2002).
[53] Xiaoliang Xu, Pei Wang, Zemin Qi *et al.*, J. Phys.: Condens. Matter **15**, L607 (2003).
[54] A. Mornel and N. EL Khiati, J. Electrochem. Soc. **140**, 2019 (1993).
[55] Y. A. Ono, *Electroluminescent Displays* (World Scientific, Singapore, 1995).
[56] R. Morimo and K. Matae, Mater. Res. Bull. **24**, 175 (1989).
[57] I. F. Chang, J. W. Brownlow, T. I. Sun, and J. S. Wilson, J. Electrochem. Soc. **136**, 3532 (1989).
[58] A. Morell and N. El Khiati, J. Electrochem. Soc. **140**, 2019 (1993).
[59] C. Barthou, J. Benoit, P. Benalloul, and A. Morell, J. Electrochem. Soc. **141**, 524 (1994).
[60] M. Cich, K. Kim, H. Choi, and S. T. Hwang, Appl. Phys. Lett. **73**, 2116 (1998).
[61] K. S. Sohn, B. Cho, and H. D. Park, J. Am. Ceram. Soc. **82**, 2779 (1999).
[62] R. Selomulya, S. Ski, K. Pita, C. H. Kam, Q. Y. Zhang, and S. Buddhudu, Mater. Sci. Eng., B **100**, 136 (2003).

This article is copyrighted as indicated in the article. Reuse of AIP content is subject to the terms at: http://scitation.aip.org/termsconditions. Downloaded to IP: 128.59.226.54 On: Wed, 10 Dec 2014 01:08:51